Supplementary Materials for

Anthropogenic warming has exacerbated droughts in southern Europe since the 1850s

Wenling An[1,2], Chenxi Xu[1,2*], Slobodan B. Marković[3,4], Shanlei Sun[5], Yue Sun[5], Milivoj B. Gavrilov[3], Zoran Govedar[6], Qingzhen Hao[1,2], Zhengtang Guo[1,2]

1. Key Laboratory of Cenozoic Geology and Environment, Institute of Geology and Geophysics, Chinese Academy of Sciences, Beijing, China

2. CAS Center for Excellence in Life and Paleoenvironment, Beijing, China

3. Faculty of Science, University of Novi Sad, Trg Dositeja Obradovića 3, 21000 Novi Sad, Serbia

4. Serbian Academy of Sciences and Arts, Belgrade, Serbia

5. Collaborative Innovation Center on Forecast and Evaluation of Meteorological Disasters/Key Laboratory of Meteorological Disaster, Ministry of Education/International Joint Research Laboratory on Climate and Environment Change, Nanjing University of Information Science & Technology (NUIST), Nanjing, China

6. Faculty of Forestry, University of Banja Luka, Banja Luka, Republic of Srpska, Bosnia and Herzegovina

*Corresponding author: Chenxi Xu, cxxu@mail.iggcas.ac.cn, †Key Laboratory of Cenozoic Geology and Environment, Institute of Geology and Geophysics, Chinese Academy of Sciences, Beijing 100029, China;

This file includes:

Supplementary Figure 1 to Supplementary Figure 12

Supplementary Table 1 to Supplementary Table 3

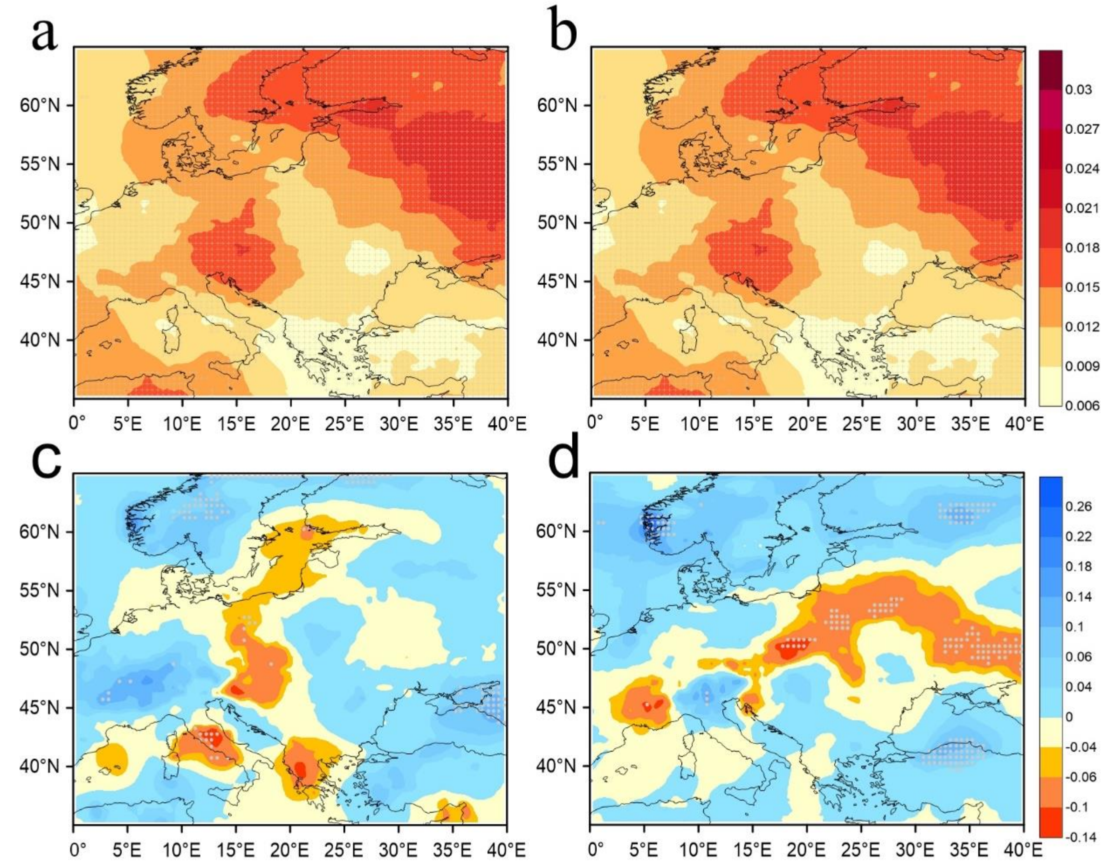

Supplementary Figure 1. Climate changes over the Europe. Mean air temperature trends for April-May (a) and June-August (b), and mean precipitation trends for April-May (c) and June-August (d), from 1901 to 2019 (the grey dots represent trends significant at the 95% confidence level).

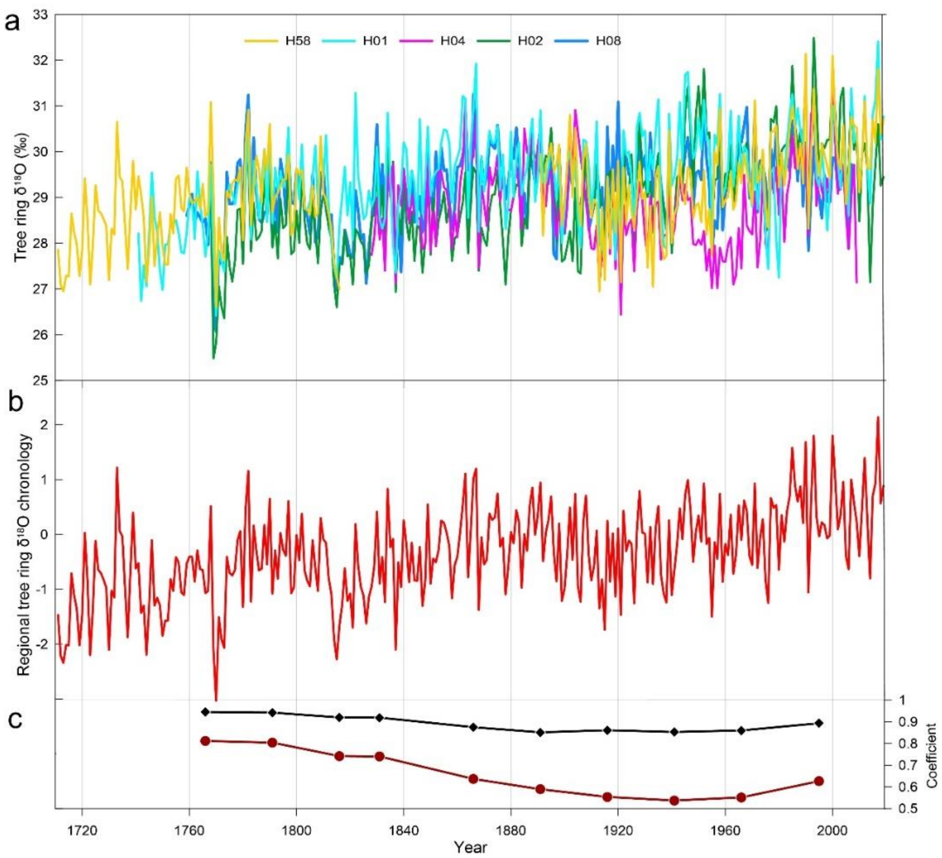

Supplementary Figure 2 Raw tree ring $\delta^{18}O$ data. The raw tree-ring $\delta^{18}O$ series of four trees (a) and (b) the final composite regional $\delta^{18}O$ chronology with running EPS (black line) and Rbar (red line) statistics used 50 yr windows, lagged 25 yr (c).

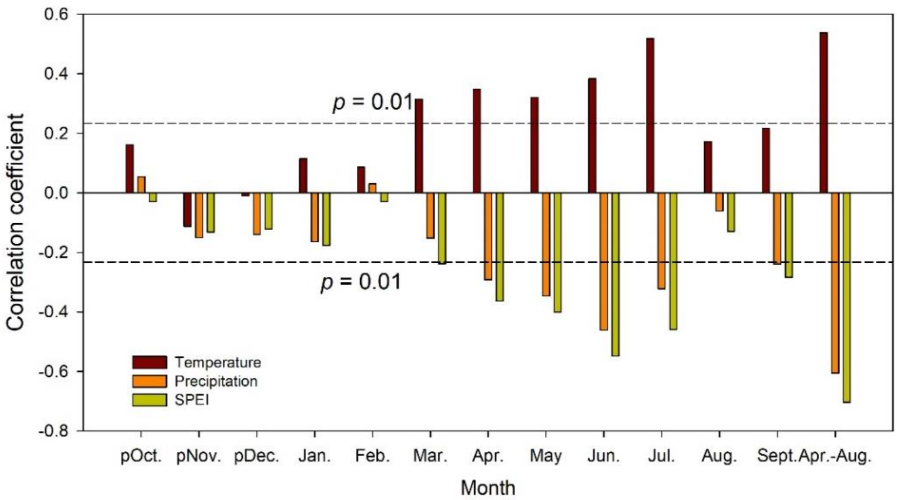

Supplementary Figure 3 Climate response of tree-ring $\delta^{18}O$ to regional climate. Correlation coefficients between tree-ring $\delta^{18}O$ and regional climatic parameters: temperature, precipitate and SPEI from 1901 to 2019. "/p" represents the values in the previous year. The dashed lines indicate that the 95% confidence interval.

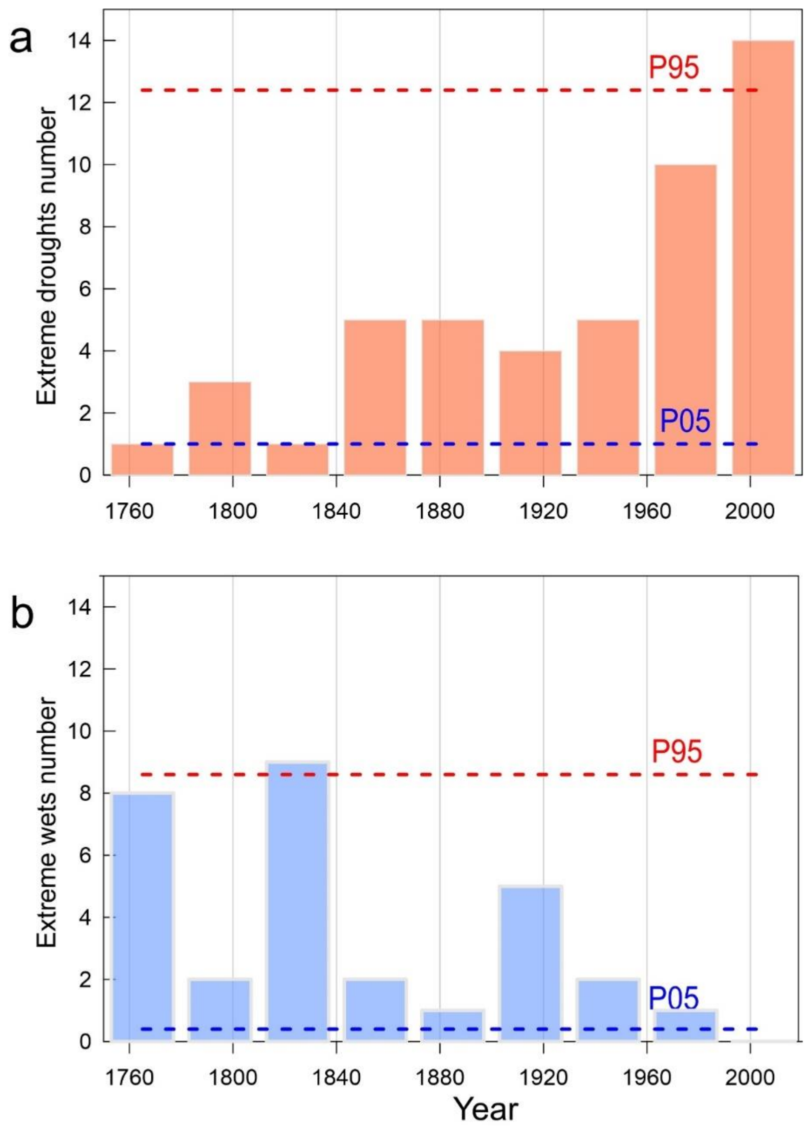

Supplementary Figure 4 Dry and wet years from southern European SPEI reconstruction. The number of extreme dry (a), and wet years (b) per 30 years (histogram), as derived from our spring-summer SPEI reconstruction. The red and black dashed lines indicate the 5% and 95% percentiles of the distribution, respectively, based on 1,000 bootstrap simulations.

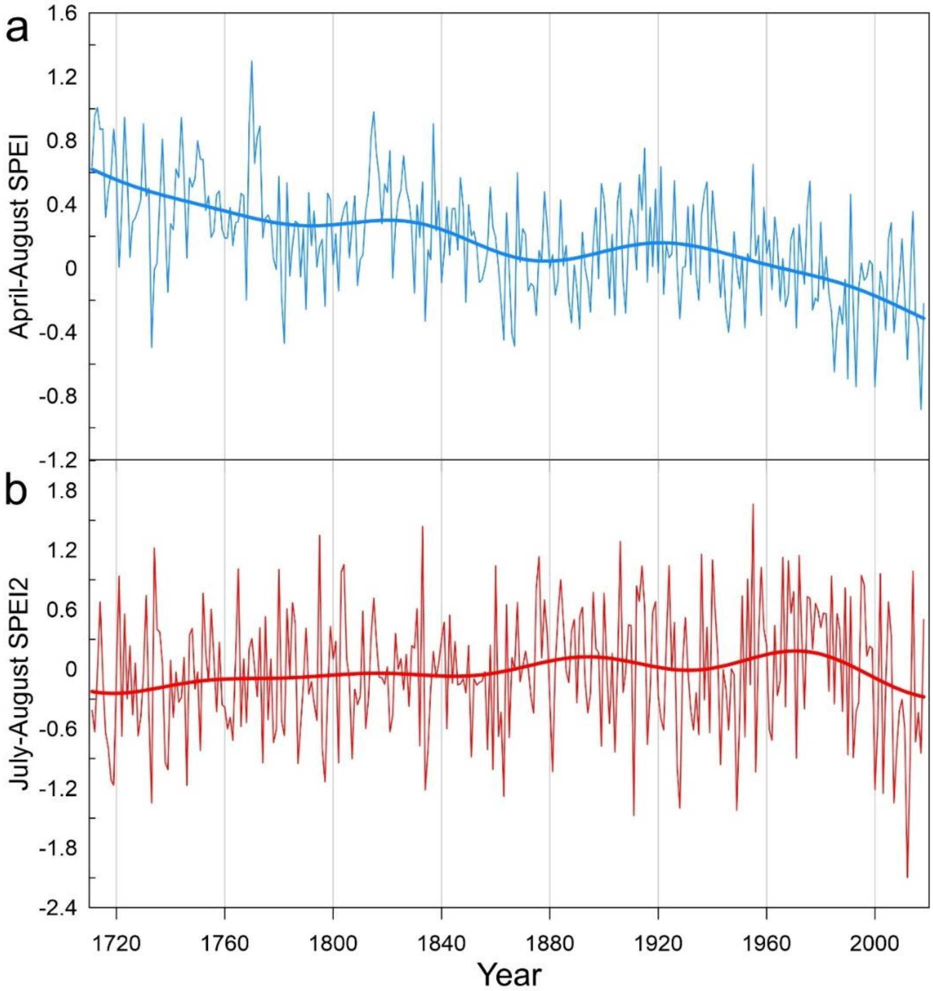

Supplementary Figure 5 SPEI reconstructions for the southern European. The April-August SPEI variations reconstruction in this study (a), and July-August SPEI variations reconstructed from the ISONET isotope data (b). The July-August SPEI2 reconstruction is obtained by averaging the gridded ISONET reconstruction for the southern Europe (about the range of 10°E-25°E, 35°N-45°N).

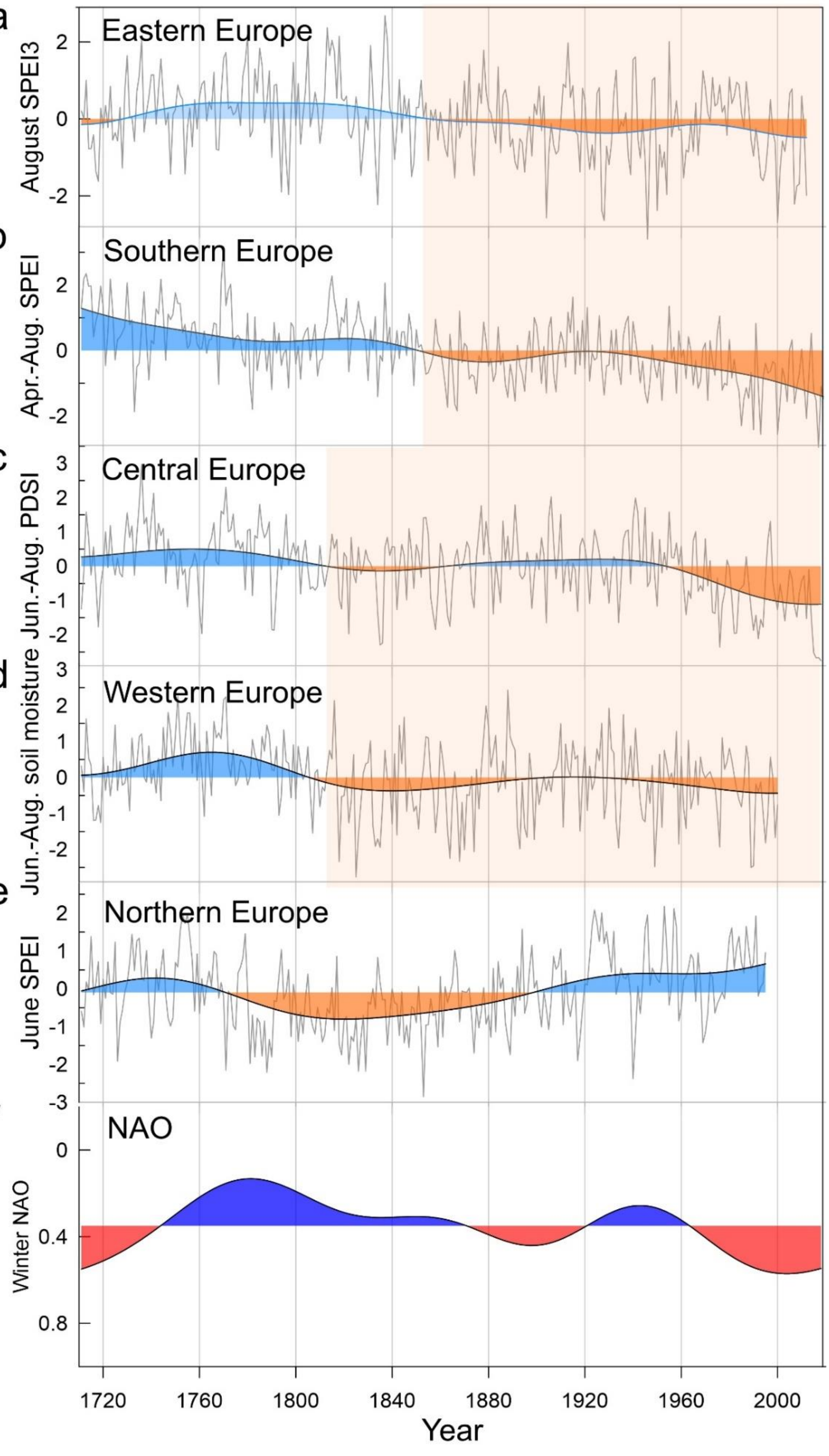

Supplementary Figure 6 Dry-wet variation records from Europe for the past 300 years. a August SPEI3 reconstruction for the eastern Europe[1]. **b** April-August SPEI reconstruction for the southern Europe (this study). **c** June-August Palmer Drought Severity Index (PDSI) reconstruction for the central Europe[2]. **d** June-August soil moisture reconstruction for the western Europe[3]. **e** June SPEI reconstruction for the northern Europe[4]. **f** winter NAO index[5], y axis was inversed for the NAO index to facilitate comparisons. The low-frequency variations in panel (a, b, c, d) are represented by the 30-yr Fast Fourier Transform (FFT) smoothing (contour area).

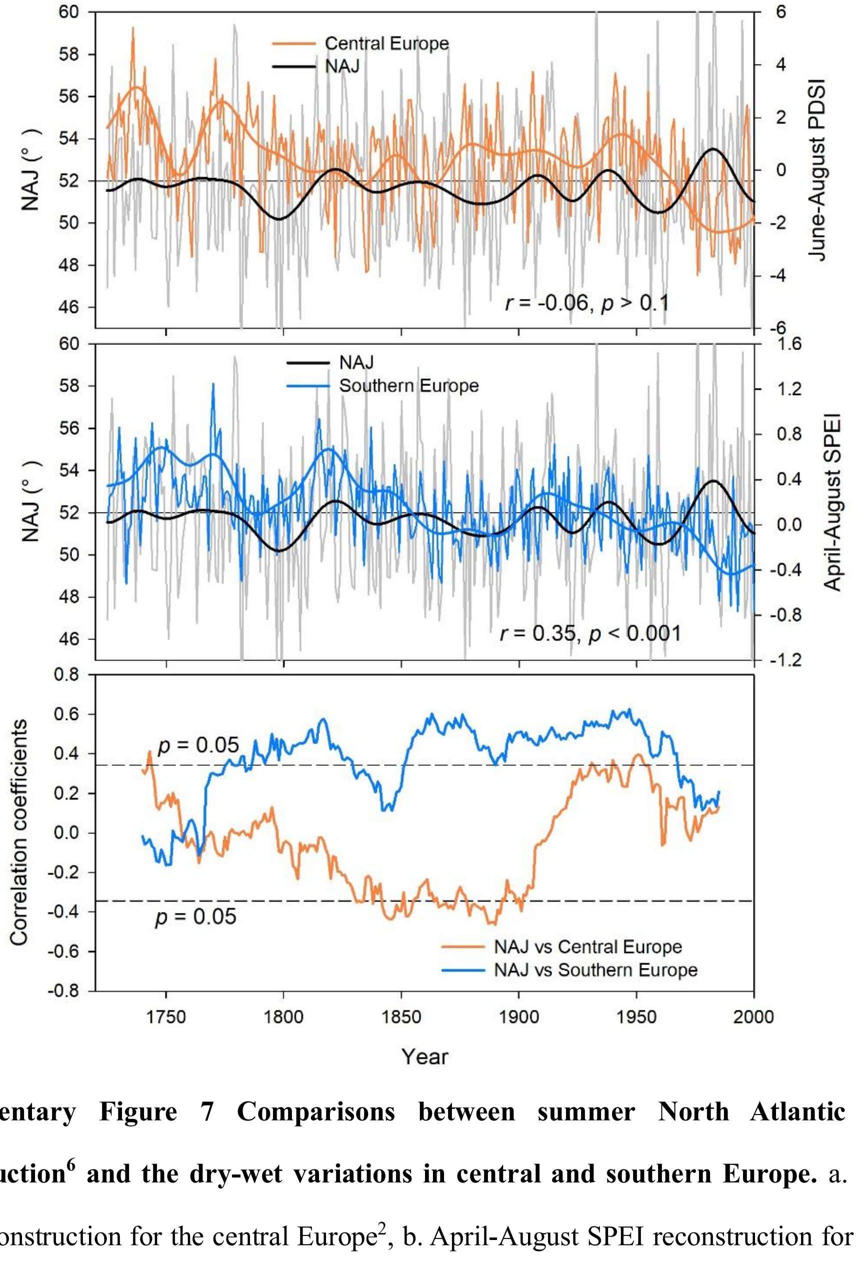

Supplementary Figure 7 Comparisons between summer North Atlantic Jet (NAJ) reconstruction[6] and the dry-wet variations in central and southern Europe. a. June-August PDSI reconstruction for the central Europe[2], b. April-August SPEI reconstruction for the southern Europe in this study. The low-frequency variations in panel (a, b) are represented by the 30-yr Fast Fourier Transform (FFT) smoothing (thick lines). c. 31-yr running correlation between summer NAJ reconstruction and dry-wet variation reconstructions for central and southern Europe.

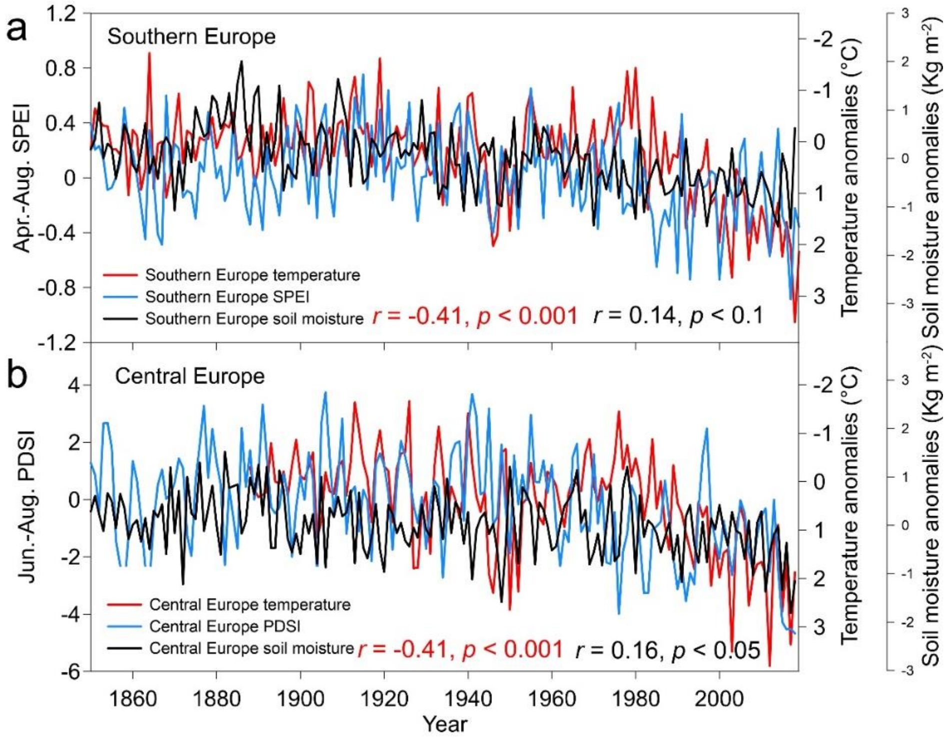

Supplementary Figure 8 Comparisons between regional climate and modelled soil moisture. The interannual variations of regional SPEI reconstruction, observed temperature from CRU dataset and soil moisture from CMIP 6 experiments under greenhouse gas (GHG) forcing for southern Europe (a) and central Europe (b). The red numbers in both panels indicate the correlation between regional SPEI and temperature, while the black numbers indicate the correlation between regional SPEI and modelled soil moisture.

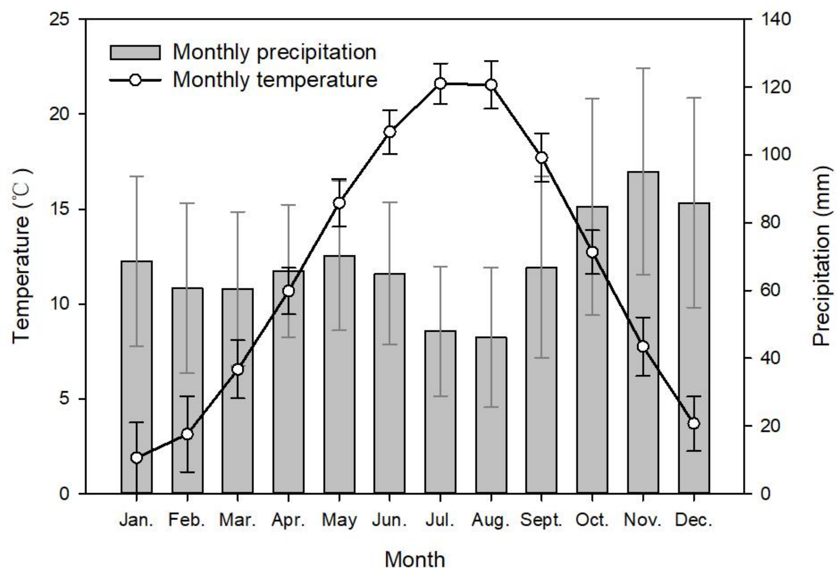

Supplementary Figure 9 Monthly climate in sampling site. Monthly precipitation, temperature for the southern Europe during the period 1901-2019, calculated from CRU dataset.

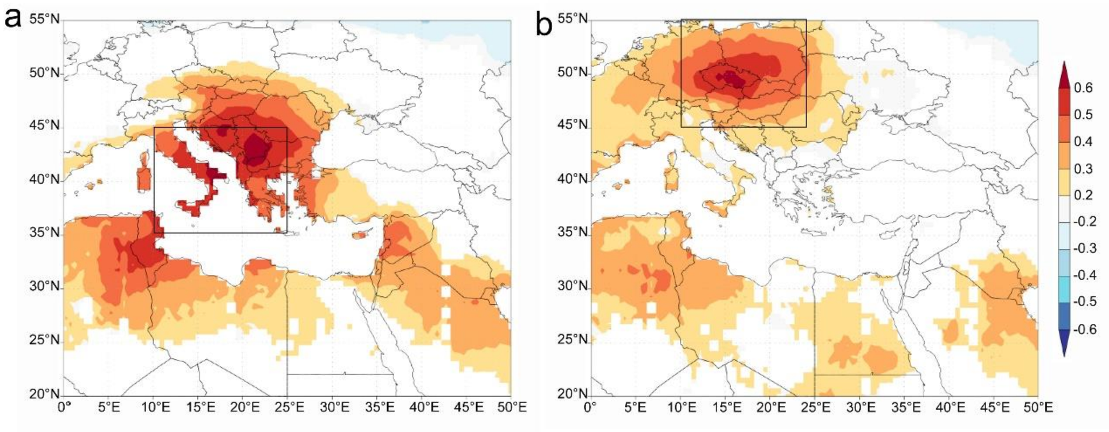

Supplementary Figure 10 Spatial representativeness of reconstructed dry-wet reconstruction. Spatial correlation coefficients (color scale) between the gridded June-August European-wide SPEI target data and the reconstructed dry-wet variation of southern (left, this study) and central Europe[2] (right) over the common period 1901–2018. The black rectangles indicate the spatial representativeness of our southern European reconstruction (about the range of 10°E-25°E, 35°N-45°N) and central European reconstruction (about the range of 10°E-25°E, 46°N-55°N).

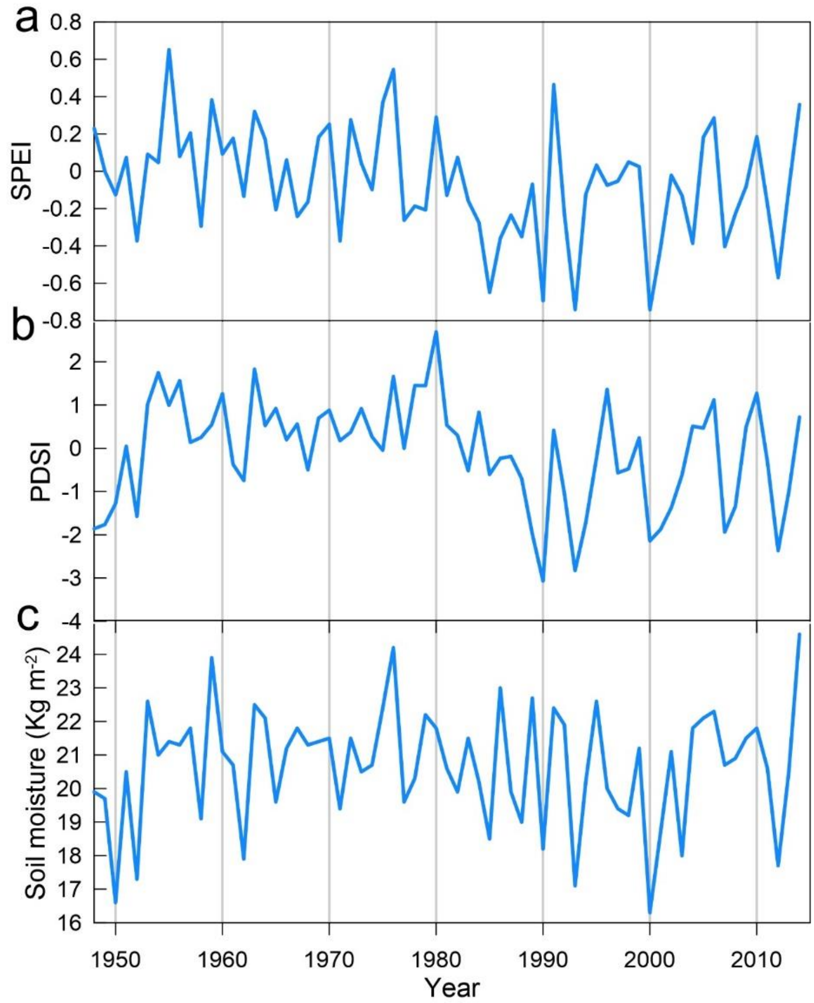

Supplementary Figure 11 Comparisons of Dry-wet index for the southern Europe. The variations of SPEI (a), PDSI (b) and soil moisture (c) for the southern Europe (about the range of 10°E-25°E, 35°N-45°N) from 1948 to 2014.

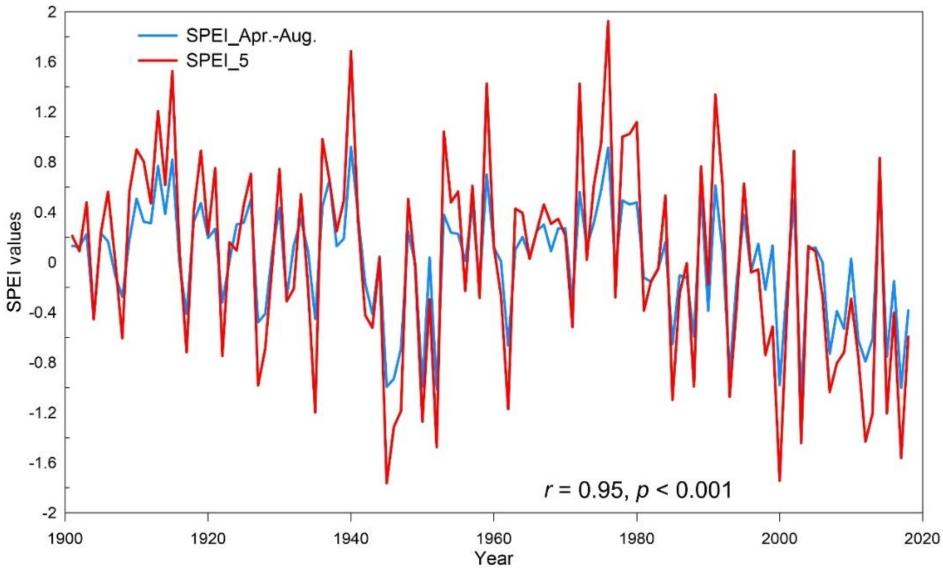

Supplementary Figure 12 Comparisons between SPEI values. The mean April–August SPEI values and the 5-month SPEI values in August variations from 1901 to 2019 for the southern Europe.

Supplementary Table 1 Information of individual trees. Correlation coefficients of tree ring $\delta^{18}O$ between four individual trees

Sample core (cover period)	H08	H02	H04	H01	H58
H08 (1759–2008)	1	0.67 ***	0.47 ***	0.65 ***	0.61***
H02 (1768–2019)		1	0.37 ***	0.66 ***	0.61 ***
H04 (1828–2009)			1	0.50 ***	0.70 ***
H01 (1740–2019)				1	0.68 ***
H58 (1711–1815, 1891-2019)					1

$^{***}p < 0.001$

Supplementary Table 2 Calibration-verification statistics. Statistics of calibration and verification for tree-ring $\delta^{18}O$ reconstruction of April-August SPEI in the common period 1901–2019 in southern Europe

Calibration		r	R^2	Durbin-Watson	verification	RE	CE	Sign test
Split/cross	1901-1959	-0.72^{***}	0.52	2.11^{*}	1960-2018	0.40	0.37	$42+/17-^{***}$
calibration-verification	1960-2019	-0.71^{***}	0.51	1.79^{*}	1901-1959	0.41	0.39	$33+/27-^{***}$

r correlation coefficient, R^2 explained variance, RE reduction of error, CE coefficient of efficiency
* $p < 0.05$; ** $p < 0.01$; *** $p < 0.001$

Supplementary Table 3 CMIP 6 Model information. Model information of the available simulations used in this study.

Model name	Spatial resolution	Analysis period	Variant label	Forcing
ACCESS-CM2	192×144	1850-2019	r1i1p1f1	NAT/GHG/ALL
ACCESS-ESM1-5	192×145	1850-2019	r1i1p1f1	NAT/GHG/ALL
BCC-CSM2-MR	320×160	1850-2019	r1i1p1f1	NAT/GHG/ALL
GFDL-ESM4	288×180	1850-2019	r1i1p1f1	NAT/GHG
GISS-E2-1-G	144×90	1850-2014	r1i1p1f1	NAT/GHG/ALL
MIROC6	256×128	1850-2019	r1i1p1f1	NAT/GHG/ALL
MRI-ESM2-0	320×160	1850-2019	r1i1p1f1	NAT/GHG/ALL
NorESM2-LM	144×96	1850-2019	r1i1p1f1	NAT/GHG/ALL
IPSL-CM6A-LR	144×143	1850-2019	r1i1p1f1	NAT/GHG/ALL

Supplementary References

1 Nagavciuc, V., Ionita, M., Kern, Z., McCarroll, D. & Popa, I. A ~700 years perspective on the 21st century drying in the eastern part of Europe based on δ18O in tree ring cellulose. *Communications Earth & Environment* **3**, doi:10.1038/s43247-022-00605-4 (2022).

2 Büntgen, U. *et al.* Recent European drought extremes beyond Common Era background variability. *Nature Geoscience*, doi:10.1038/s41561-021-00698-0 (2021).

3 Wang, L. *et al.* The 1820s Marks a Shift to Hotter ‐ Drier Summers in Western Europe Since 1360. *Geophys. Res. Lett.* **49**, doi:10.1029/2022gl099692 (2022).

4 Seftigen, K., Goosse, H., Klein, F. & Chen, D. Hydroclimate variability in Scandinavia over the last millennium – insights from a climate model–proxy data comparison. *Climate of the Past* **13**, 1831-1850, doi:10.5194/cp-13-1831-2017 (2017).

5 Cook, E. R. *et al.* A Euro-Mediterranean tree-ring reconstruction of the winter NAO index since 910 C.E. *Climate Dynamics* **53**, 1567-1580, doi:10.1007/s00382-019-04696-2 (2019).

6 Trouet, V., Babst, F. & Meko, M. Recent enhanced high-summer North Atlantic Jet variability emerges from three-century context. *Nat Commun* **9**, 180, doi:10.1038/s41467-017-02699-3 (2018).